

RESEARCH ARTICLE

NEUROSCIENCE

Rapid eye movement sleep is initiated by basolateral amygdala dopamine signaling in mice

Emi Hasegawa^{1,2}, Ai Miyasaka¹, Katsuyasu Sakurai¹, Yoan Cherasse¹, Yulong Li³, Takeshi Sakurai^{1,2,4*}

The sleep cycle is characterized by alternating non-rapid eye movement (NREM) and rapid eye movement (REM) sleeps. The mechanisms by which this cycle is generated are incompletely understood. We found that a transient increase of dopamine (DA) in the basolateral amygdala (BLA) during NREM sleep terminates NREM sleep and initiates REM sleep. DA acts on dopamine receptor D2 (Drd2)-expressing neurons in the BLA to induce the NREM-to-REM transition. This mechanism also plays a role in cataplectic attacks—a pathological intrusion of REM sleep into wakefulness—in narcoleptics. These results show a critical role of DA signaling in the BLA in initiating REM sleep and provide a neuronal basis for sleep cycle generation.

Sleep-wakefulness states are influenced by noradrenergic neurons in the locus coeruleus, histaminergic neurons in the tuberomammillary nucleus, and serotonergic neurons in the dorsal raphe, all of which share similar firing patterns—with rapid firing during wakefulness, slow and occasional firing during non-rapid eye movement (NREM) sleep, and almost complete cessation of firing during rapid eye movement (REM) sleep (1, 2). However, dopaminergic neurons in the ventral tegmental area (VTA) (DA^{VTA} neurons) were reported to show different firing patterns from those of other monoaminergic neurons (3–5). A recent fiber-photometry study showed that DA^{VTA} neurons exhibited lower activity during NREM sleep than during either wakefulness or REM sleep. The activity of these neurons began to increase before the NREM-to-REM and NREM-to-wakefulness transitions (6). Tracing studies revealed that DA^{VTA} neurons are composed of heterogeneous populations with different input and output organizations (7, 8), which suggests the possible existence of multiple DA^{VTA} neuronal populations with distinct firing patterns across sleep-wakefulness states. In this study, we examined extracellular dopamine (DA) levels across the sleep-wakefulness cycle in several brain regions that receive dense projections of DA^{VTA} neurons, using a G protein-coupled receptor (GPCR) activation-based (GRAB) sensor for DA (GRAB_{DA}) (9) to determine the existence of subpopulations of DA^{VTA} neurons with differential roles in sleep-wakefulness regulation.

DA level in the basolateral amygdala increases before NREM-to-REM sleep transitions

We expressed GRAB_{DA} in the basolateral amygdala (BLA), the nucleus accumbens (NAc), the medial prefrontal cortex (mPFC), or the lateral hypothalamic area (LHA) of mice and implanted optical fibers for photometry to examine the relationship between DA levels and each sleep-wakefulness state transition (Fig. 1 and fig. S1). We found three patterns of DA dynamics during the NREM-to-REM transition. DA levels in the BLA showed a characteristic pattern with a transient increase that started just before each NREM-to-REM transition and a decrease during REM sleep (Fig. 1, A to D). DA elevation started earlier than the NREM-to-REM sleep transition. In the NAc, DA levels also showed an elevation before the NREM-to-REM sleep transition and a fluctuation with a slightly higher mean value during REM sleep (Fig. 1, E to H). The mPFC and LHA shared similar temporal patterns of DA levels, with a robust decrease during REM sleep without a prior increase in DA level (Fig. 1, I to P). Levels of noradrenaline (NA) and serotonin [5-hydroxytryptamine (5-HT)] in the BLA showed completely different patterns from those of DA (fig. S2).

Next, we examined the effect of DA increase in the BLA and NAc during NREM sleep on sleep-wakefulness states. We expressed stabilized step function opsin (SSFO) (10) in DA^{VTA} neurons in *DAT-ires-Cre* mice (Fig. 2, A and H) and implanted optical fibers in the BLA or NAc bilaterally (fig. S3A) for optogenetic stimulation (1-s width). Excitation of DA fibers in the BLA during NREM sleep caused a transition to REM sleep (Fig. 2, B and C). REM sleep started 142.4 ± 33.7 s after stimulation, which was significantly earlier than observed in the control group (Fig. 2C). Excitation of DA fibers in the BLA every 30 min from zeitgeber time 8 (ZT8) to ZT11 robustly increased REM sleep at

the expense of NREM sleep (Fig. 2, D and E, and table S1). The electroencephalography (EEG) power spectrum during each state was not significantly changed by the optogenetic manipulation of DA fibers in the BLA (Fig. 2F). Duration of NREM sleep was shortened because NREM sleep bouts were terminated earlier by the optogenetic stimulation (Fig. 2G).

By contrast, excitation of DA fibers in the NAc during NREM sleep did not cause state transition (Fig. 2, I and J). Shining a light (for 1 s) every 30 min resulted in a slight increase of NREM sleep time at the expense of wakefulness time (Fig. 2, K and L), which is consistent with a previous result that found that excitation of direct pathway neurons in the NAc decreased wakefulness (11). However, this manipulation did not influence REM sleep. Excitation of DA fibers in the mPFC or LHA also did not affect the amount of each state (fig. S4 and table S2).

These observations showed that a transient DA increase in the BLA caused the NREM-to-REM sleep transition. Supporting this, optogenetic inhibition of DA^{VTA} fibers in the BLA lengthened latency to REM sleep and decreased REM sleep amount (Fig. 3, A to E, and table S1) without affecting the EEG power spectrum (Fig. 3F).

Dopamine receptor D2-positive neurons in the BLA trigger NREM-to-REM transition

Complete DA depletion abolished REM sleep in mice, and treatment with a dopamine receptor D2 (Drd2) agonist restored REM sleep (12). Moreover, in rodents, low doses of a Drd2 agonist increased REM sleep, although larger doses of a Drd2 agonist reduced REM sleep, presumably as a result of presynaptic inhibition of DA release (13). These findings suggest the involvement of Drd2 in REM sleep regulation, consistent with the evidence that blockade of Drd2 decreases REM sleep (14). Furthermore, injection of a Drd2 agonist into the amygdala increased REM sleep in rats (15). When considered in conjunction with the fiber-photometry data (Fig. 1), these observations lead us to hypothesize that DA acts on Drd2-positive neurons in the BLA to initiate REM sleep. To examine the effect of DA on Drd2 neurons in the BLA, we performed an electrophysiological study. After expressing SSFO in DA^{VTA} neurons in *Drd2-Cre; DAT-ires-Cre* (Drd2/DAT-Cre) mice, we prepared brain slices and subjected them to whole-cell recordings from Drd2-positive neurons in the BLA (Fig. 4A). Excitation of DA fibers by application of light (1 s) induced long-lasting hyperpolarization, which was blocked by a Drd2 antagonist. This suggests that DA inhibited Drd2 neurons in the BLA through Drd2 (Fig. 4, B to D).

Because DA induced hyperpolarization of Drd2 neurons in the BLA, we next examined whether optogenetic inhibition of these cells

¹International Institute for Integrative Sleep Medicine (WPI-IIIS), University of Tsukuba, Tsukuba, Ibaraki 305-8575, Japan.

²Faculty of Medicine, University of Tsukuba, Tsukuba, Ibaraki 305-8575, Japan. ³State Key Laboratory of Membrane Biology, Peking University School of Life Sciences, Beijing 100871, China. ⁴Life Science Center for Tsukuba Advanced Research Alliance (TARA), University of Tsukuba, Tsukuba, Ibaraki 305-8575, Japan.

*Corresponding author. Email: sakurai.takeshi.gf@u.tsukuba.ac.jp

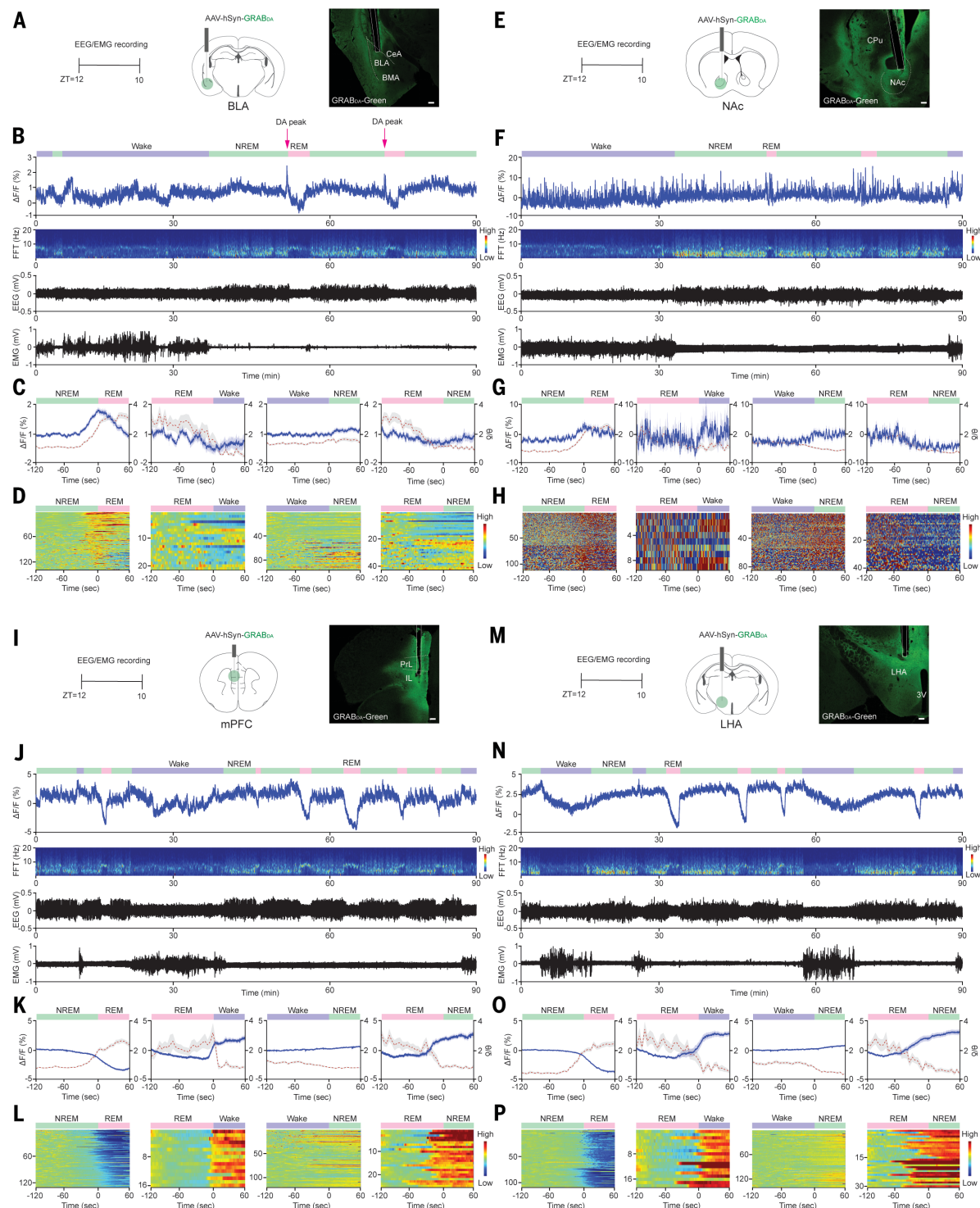


Fig. 1. Temporal changes of DA levels in brain regions across each vigilance state. (A, E, I, and M) (Left) Experimental designs. (Middle) Fiber locations and adeno-associated virus (AAV) injection. (Right) Representative coronal brain sections stained with anti-green fluorescent protein (GFP) (green) antibody. The white lines mark the positions of the optical fibers. Scale bars, 100 μ m. BMA, basomedial amygdala; CPu, caudate putamen; PrL, prelimbic cortex; IL, infralimbic cortex; 3V, third ventricle. (B, F, J, and N) (Top) Representative traces of DA levels in the BLA (B), NAc (F), mPFC (J), and LHA (N) in C57BL/6J mice. Purple, green, and pink bars show wakefulness, NREM sleep, and REM

sleep, respectively. (Middle and bottom) Time-resolved power spectra and waveforms of EEG and electromyography (EMG). $\Delta F/F$, change in fluorescence intensity; FFT, fast Fourier transform. (C, G, K, and O) Temporal changes in DA levels at each transition (blue) and theta/delta ratios (red dotted lines) (averages \pm SEMs). Time is relative to the transition of states. (D, H, L, and P) Heatmaps showing DA level at each transition (3 mice, recorded for 22 hours). Only state transitions where the preceding state lasted >120 s and another state after it lasted >60 s were extracted and converted to data. The numbers of data for each state transition extracted from each mouse are shown in table S6.

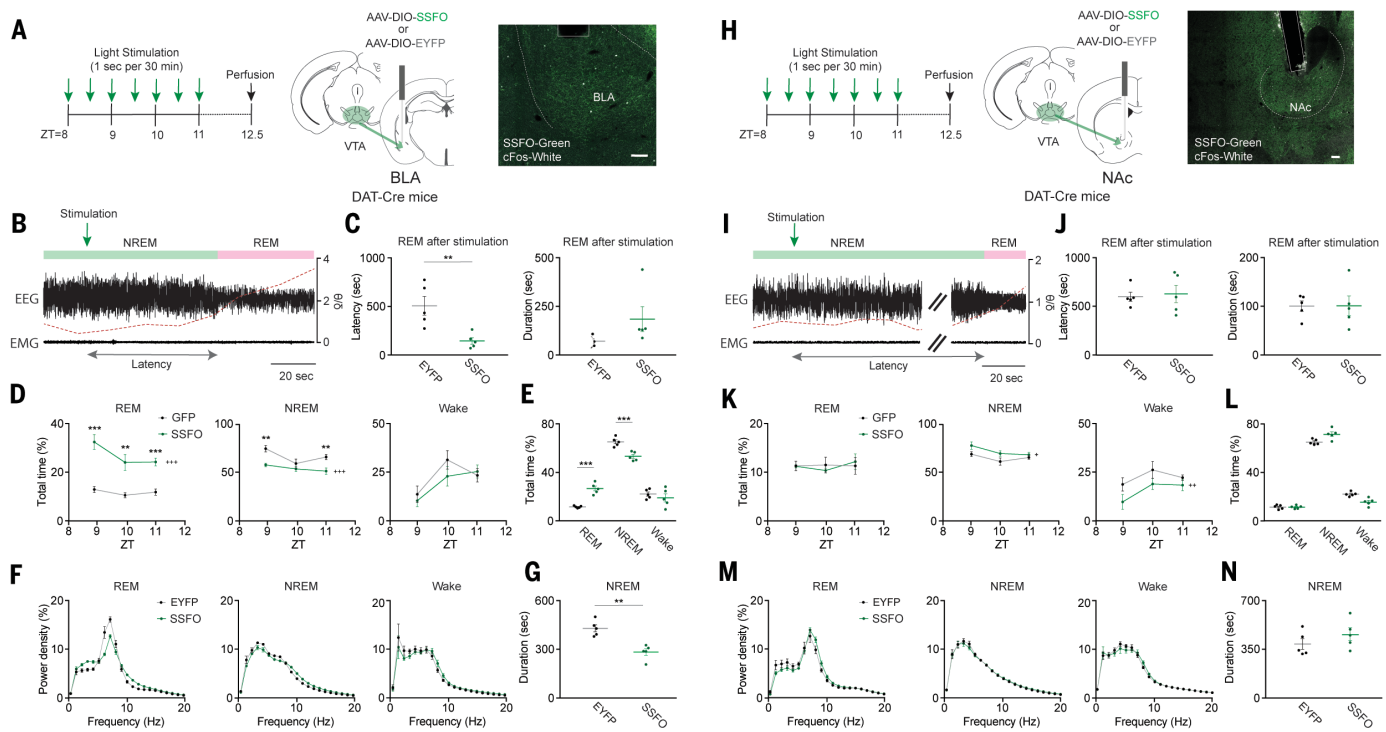


Fig. 2. Optogenetic excitation of DA^{VTA} fibers in the BLA during NREM sleep induces REM sleep. (A and H) (Left) Experimental designs. (Middle) Schematic drawings of fiber placement and AAV injection. (Right) Coronal brain sections stained with anti-GFP (green) and anti-cFos (white) antibodies. The white lines mark the positions of optical fibers. Scale bars, 100 μ m. **(B and I)** Representative traces of EEG and EMG and theta/delta ratios in DAT-ires-Cre mice expressing SSFO in DA^{VTA} neurons and implanted optical fibers in the BLA (B) or NAc (I) (bilateral). Arrows show time of light stimulation. Green and pink bars represent time of NREM and REM sleep, respectively. **(C and J)** REM latency and duration after first light

stimulation. **(D and K)** Hourly amounts of REM sleep (REM), NREM sleep (NREM), and wakefulness (wake) with light stimulation in the BLA (D) or NAc (K) for ZT8 to ZT11. **(E and L)** Total amount of REM sleep (REM), NREM sleep (NREM), and wakefulness (wake) in ZT8 to ZT11. **(F and M)** Power spectra of EEG frequency during each state in ZT8 to ZT11. **(G and N)** Duration of NREM in ZT8 to ZT11. Data are from DAT-ires-Cre mice expressing SSFO or EYFP in DA^{VTA} neurons with photostimulation in the BLA or NAc (SSFO, $n = 5$, $n = 5$; EYFP, $n = 5$, $n = 5$) [${}^*P < 0.05$, ${}^{**}P < 0.01$, ${}^{***}P < 0.001$, unpaired t test; ${}^{++}P < 0.001$, two-way repeated measures analysis of variance (ANOVA)].

induced REM sleep. We expressed vertebrate low-wavelength opsin (vLWO), which, like Drd2, couples to the Gi subclass of G proteins and induces hyperpolarization by light (16) in Drd2 neurons in the BLA of *Drd2-Cre* mice (Fig. 4E). Whole-cell recordings using slice preparations showed that shining a light pulse (462 nm, 1 Hz, 40 s) caused long-lasting hyperpolarization of enhanced yellow fluorescent protein (EYFP)-positive neurons, similar to the hyperpolarization observed when DA fibers were excited (Fig. 4, F to H). We next implanted optical fibers in the BLA in *Drd2-Cre* mice expressing vLWO and optogenetically inhibited Drd2 neurons (Fig. 4I). Application of a light pulse during NREM sleep caused a transition to REM sleep (Fig. 4J). REM sleep started 89.2 ± 20.3 s after manipulation, which was significantly earlier than in the control group expressing only EYFP (Fig. 4K). Application of a light pulse every 30 min starting from ZT8 to ZT11 increased the amount of REM sleep and decreased NREM sleep (Fig. 4, L and M, and table S3) without affecting the EEG power spectrum (Fig. 4N). Duration of NREM sleep was shortened

(Fig. 4O). Fos expression was increased in the cell population around EYFP-expressing cells in the BLA but not in EYFP-expressing cells (Fig. 4P), which suggests that inhibition of Drd2 cells caused disinhibition of BLA neurons. These activated neurons in the amygdala send specific projections to the mesopontine junction regions that are implicated in the REM regulation (fig. S5).

Chemogenetic inhibition of Drd2 neurons in the BLA of *Drd2-Cre* mice increased REM sleep time and decreased NREM sleep time (Fig. 4, Q to S, and table S4), further supporting the importance of Drd2 neurons in the BLA in triggering REM sleep. We again observed an increase of Fos-positive neurons in the BLA as well as in the central nucleus of the amygdala (CeA) (Fig. 4T).

Axonal projections by Drd2 neurons in the BLA were almost exclusively observed in the BLA (fig. S6A), which suggests that Drd2 neurons in the BLA mainly act inside the BLA. An electrophysiological study also showed that optogenetic inhibition of Drd2 neurons in the BLA excited neurons other than Drd2-positive cells (fig. S6, B to G).

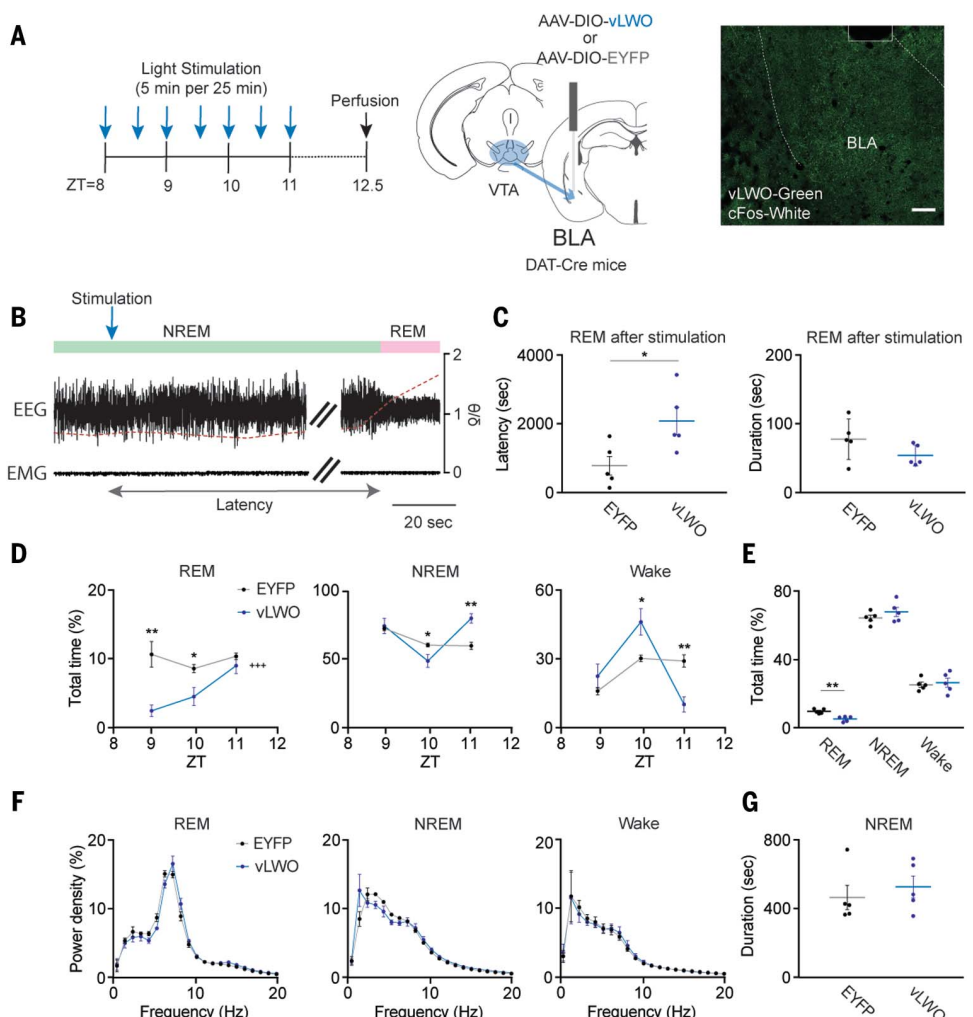
Transient DA increase in the BLA during wakefulness induces cataplexy

We next examined whether DA signaling in the BLA is also involved in the emergence of cataplexy, which is a pathological intrusion of REM sleep into wakefulness. A previous study had shown that Drd2 agonists or antagonists increased or decreased cataplexy, respectively, in narcoleptic dogs and mice (17–19).

We expressed GRAB_{DA} in the BLA of narcoleptic *orexin-ataxin 3* mice (20) and implanted an optical fiber to examine the relationship between DA level and cataplexy (Fig. 5A and fig. S1C). We fed mice chocolate to increase the number of cataplexy episodes (21). Cataplexy-like episodes (CLEs), characterized by abruptly occurring behavioral arrest (22), were observed in *orexin-ataxin 3* mice (20) but never in wild-type littermates. We observed a transient increase in DA levels while eating chocolate, which was followed by CLEs (Fig. 5B and movie S1). The increment of DA level in the BLA during chocolate feeding in *orexin-ataxin 3* mice (5.8 ± 0.005) was larger than that observed in control mice (1.7 ± 0.002 ; $P < 0.001$, unpaired t test) (Fig. 5, B and C). By contrast,

Fig. 3. Inhibition of DA^{VTA} fibers in the BLA decreases REM sleep.

(A) Experimental design. (Middle) Fiber placement and AAV injection in the BLA. (Right) Coronal brain section stained with anti-GFP (green) and anti-cFos (white) antibodies in the amygdala. The white line marks the position of the optical fiber. Scale bar, 100 μ m. **(B)** Representative traces of EEG and EMG and theta/delta ratio in a DAT-ires-Cre mouse expressing vLWO in DA^{VTA} neurons and implanted optical fibers in the BLA (bilateral). The blue arrow shows time of light stimulation, and the green and pink bars represent time of NREM and REM sleep, respectively. **(C)** REM latency and duration after first light stimulation. **(D)** Amount of REM sleep (REM), NREM sleep (NREM), and wakefulness (wake) per 1 hour with light stimulation in ZT8 to ZT11. **(E)** Total amount of each state in ZT8 to ZT11. **(F)** Power spectra of EEG frequency during each state in ZT8 to ZT11. **(G)** Duration of NREM sleep in ZT8 to ZT11. Data are from DAT-ires-Cre mice expressing vLWO or EYFP in DA^{VTA} neurons with photostimulation in the BLA (vLWO, $n = 5$; EYFP, $n = 5$) (relative to EYFP, * $P < 0.05$, ** $P < 0.01$, *** $P < 0.001$, unpaired t test; +++ $P < 0.001$, two-way repeated measures ANOVA).



the amplitudes of DA increase in the NAc during chocolate feeding were similar in narcoleptic and control mice (fig. S7).

Next, we expressed SSFO in DA^{VTA} neurons in DAT-ires-Cre mice and implanted optical fibers in the VTA for optogenetic excitation during wakefulness (Fig. 5D). We simultaneously monitored DA level in the BLA. Application of laser for 1 s, which was accompanied by Fos expression in SSFO-positive cells in the VTA (Fig. 5D), caused a transient increase in DA level with a similar pattern to that observed during chocolate feeding in narcoleptic mice preceding cataplexy (Fig. 5, B and E). The increase of DA level was followed by CLEs, even in DAT-ires-Cre mice in which orexin peptides were produced (movie S2). We next examined the effects of stimulation of DA^{VTA} fibers in the BLA, NAc, mPFC, or LHA (fig. S3D) and found that optogenetic excitation during wakefulness caused CLEs only when optical fibers were implanted in the BLA (fig. S8, A to E).

We next expressed vLWO in Drd2 neurons in the BLA of Drd2-Cre mice and implanted optical fibers in the BLA (Fig. 5F). Optogenetic inhibition by applying a light pulse (1 Hz,

1 min) during wakefulness caused CLEs (Fig. 5, G and H). The EEG power spectrum during the induced CLEs was similar to that observed during cataplexy in orexin-ataxin 3 mice (Fig. 5H). After optogenetic inhibition, we observed an increase in Fos-positive neurons in the BLA (Fig. 5I). We next injected AAV-DIO-hM4Di-mCherry into the BLA of Drd2-Cre;orexin-ataxin 3 mice (Drd2/ataxin 3 mice) to examine the effect of chemogenetic inhibition of Drd2-positive neurons in the BLA on cataplexy (Fig. 5J). Clozapine-N-oxide (CNO) administration increased the total time and number of cataplexy episodes (Fig. 5, K and L, and table S5). Administration of CNO caused an increase in Fos-positive neurons in the BLA and CeA (Fig. 5M). Moreover, optogenetic inhibition of DA^{VTA} fibers in the BLA almost completely abolished the occurrence of CLEs in DAT-ires-Cre;orexin-ataxin 3 mice (fig. S8, F and G).

Discussion

The amygdala plays a crucial role in processing emotional signals during wakefulness. However, neuroimaging and intracranial recording studies have shown amygdala activation dur-

ing REM sleep in humans (23, 24). We show that a transient increase in DA levels in the BLA during NREM sleep terminates NREM sleep and starts REM sleep. Drd2-positive neurons in the BLA play a pivotal role in this process through the disinhibition of BLA neurons. The increment of DA in these peaks showed only a weak correlation with the length of inter-REM intervals that preceded the DA peak as well as the REM sleep duration that followed, which suggests that the DA peak at the transition does not play a major role in the homeostatic regulation of REM sleep (fig. S9).

Retrograde tracing with RetroBeads injected into the BLA and NAc in wild-type mice showed no double-positive cells in the VTA (fig. S10, A to D). Injection of AAV₂retro-DIO-ChR2-EYFP into the NAc of DAT-ires-Cre mice to label the DA^{VTA} neurons that send innervations to the NAc showed that channelrhodopsin-2 (ChR2)-positive fibers were observed in the NAc and LHA but not in the BLA (fig. S10, E and F). These observations suggest that DA^{VTA} populations sending projections to the BLA and NAc are distinct. DA^{VTA} neurons that send

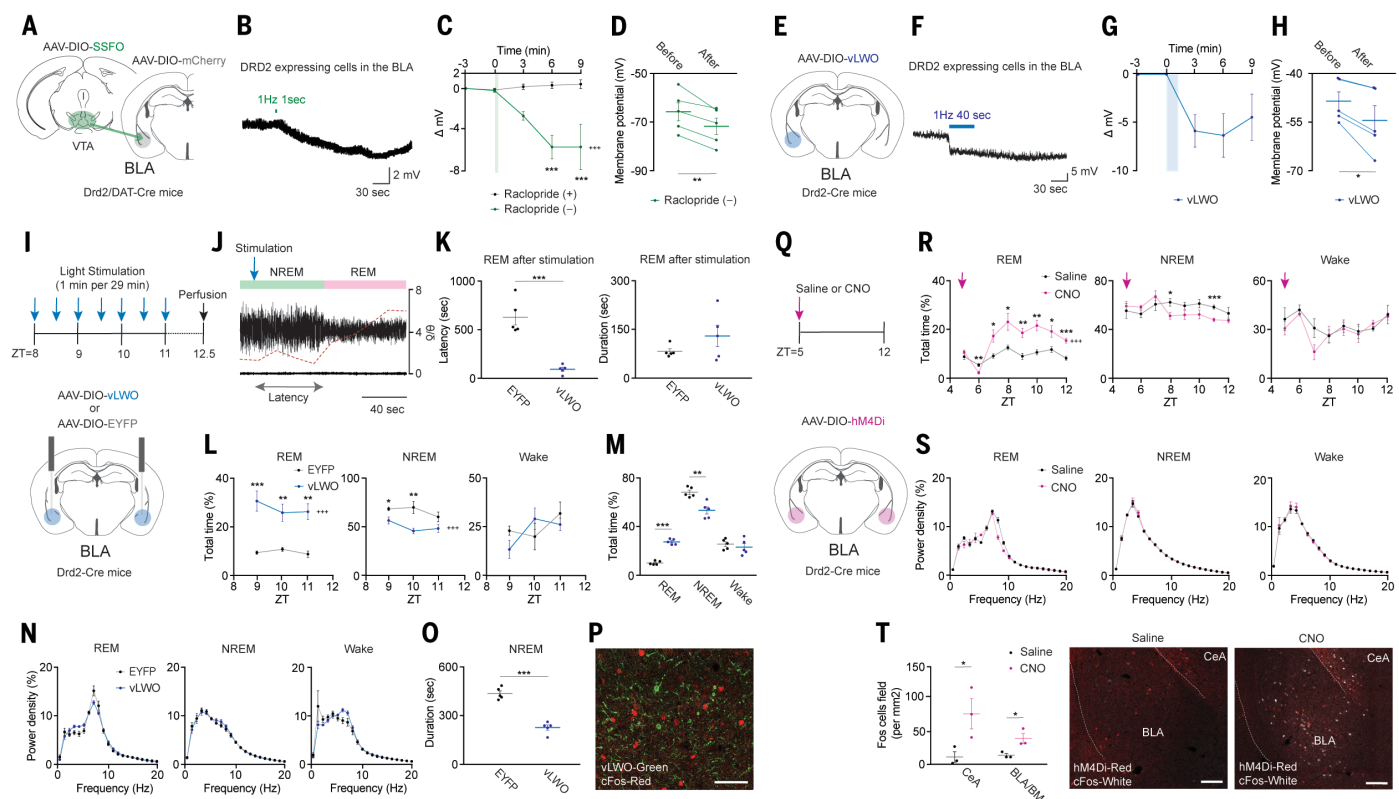


Fig. 4. Drd2-positive neurons in the BLA mediate the NREM-to-REM sleep transition. (A and E) Schematic drawings of experimental design. (B and F) Traces of current clamp recording from Drd2-positive cells in the BLA. Green and blue bars show time of light stimulation of DA^{VTA} axon terminals (B) or Drd2-positive cells (F). (C, D, G, and H) Hyperpolarization of Drd2-positive cells relative to baseline. Before indicates the average for 3 min before light stimulation, and after indicates the average for 3 to 6 min after light stimulation (*P < 0.05, Mann-Whitney test or paired t test; n = 5). (B), (C), and (D) were done under the presence of GABA_A and/or raclopride. (I) (Top) Experimental design. (Bottom) Schematic drawing of fiber locations and AAV injection in the BLA. (J) Representative EEG and EMG traces and theta/delta ratio of EEG in Drd2-Cre mice expressing vLWO in Drd2-positive cells in the BLA and implanted optical fibers in the BLA (bilateral). The blue arrow shows time of light stimulation, and green and pink bars represent NREM and REM sleep, respectively. (K) REM latency and duration after first light stimulation. (L) Hourly amount of REM sleep (REM), NREM sleep (NREM), and wakefulness (wake) with light stimulation. (M) Total amount of each state in ZT8 to ZT11. (N) Power

spectra of EEG frequency during each state in ZT8 to ZT11. (O) Duration of NREM sleep in ZT8 to ZT11. Drd2-Cre mice expressed vLWO or EYFP in the amygdala with photostimulation in the BLA (vLWO, n = 5; EYFP, n = 5) (relative to EYFP, *P < 0.05, **P < 0.01, ***P < 0.001, unpaired t test; +++P < 0.001, two-way repeated measures ANOVA). (P) Coronal brain section stained with anti-GFP (green) and anti-cFos (red) antibodies in the amygdala. Scale bar, 100 μm. (Q) (Top) Experimental design. (Bottom) Schematic drawing of AAV injection in the BLA. (R) Hourly amount of each state after administration of saline or CNO in ZT5 to ZT12. Arrows show the administration of saline or CNO at ZT5 (relative to saline, *P < 0.05, **P < 0.01, ***P < 0.001, paired t test; +++P < 0.001, two-way repeated measures ANOVA). (S) Power spectra of EEG frequency during each state in ZT5 to ZT12. (T) (Left) Number of Fos-positive cells in the CeA and the BLA or BMA after administration of saline or CNO (saline, n = 3; CNO, n = 3) (*P < 0.05, unpaired t test). (Right) Coronal brain sections stained with anti-mCherry (red) and anti-cFos (white) antibodies in the amygdala. Scale bars, 100 μm. Data are from Drd2 mice expressing hM4Di mCherry (n = 6).

innervations to the BLA localize in the dorsal regions, whereas populations that send projections to the NAc were found in the ventral part of the VTA.

In vitro electrophysiological studies suggested that DA- or vLWO-mediated inhibition of Drd2 neurons in the BLA caused long-lasting hyperpolarization (Fig. 4, C and G). This long-lasting hyperpolarization might be a characteristic of this group of neurons when Gi proteins are activated and might be involved in the mechanism that maintains the stability of REM sleep. Mimicking long-lasting inhibition of BLA Drd2 by designer receptors exclusively activated by designer drugs (DREADD) increased REM sleep in wild-type mice and

catalepsy in narcoleptic mice, supporting this hypothesis (Fig. 4, Q and R, and Fig. 5, J and K).

We also found that the DA peak in the BLA preceded cataleptic attacks in narcoleptic mice. Mimicking the DA increase in the BLA induced muscle atonia with behavioral arrests in mice, which were similar to the behaviors observed in cataplexy (Fig. 5, D and E). In this study, we used SSFO for optogenetic excitation of DA^{VTA} neurons because excitation of DA^{VTA} neurons with SSFO by applying a 1-s light pulse caused transient excitation of DA^{VTA} neurons (fig. S11) along with transient DA elevation in the BLA (Fig. 5E), which was similar to the pattern of DA increase before the NREM-to-REM transitions (Fig. 1, A to D). DA

reuptake inhibitors, which are used for the treatment of narcolepsy, had no effect on catalepsy or REM sleep (25), which suggests that transient increase, but not sustained elevation of DA levels, triggers REM sleep or cataplexy.

In narcoleptic patients, cataplexy is often triggered by positive emotion and amygdala activity increases in cataplexy (26), which suggests roles of the amygdala and reward system in cataplexy (27–29). We found that DA levels in the BLA transiently increased before cataplexy attacks in narcoleptic mice but not in wild-type mice (Fig. 5). Positive emotion might induce a transient increase of DA in the BLA in narcoleptics but not in wild types, mimicking the DA dynamics that trigger

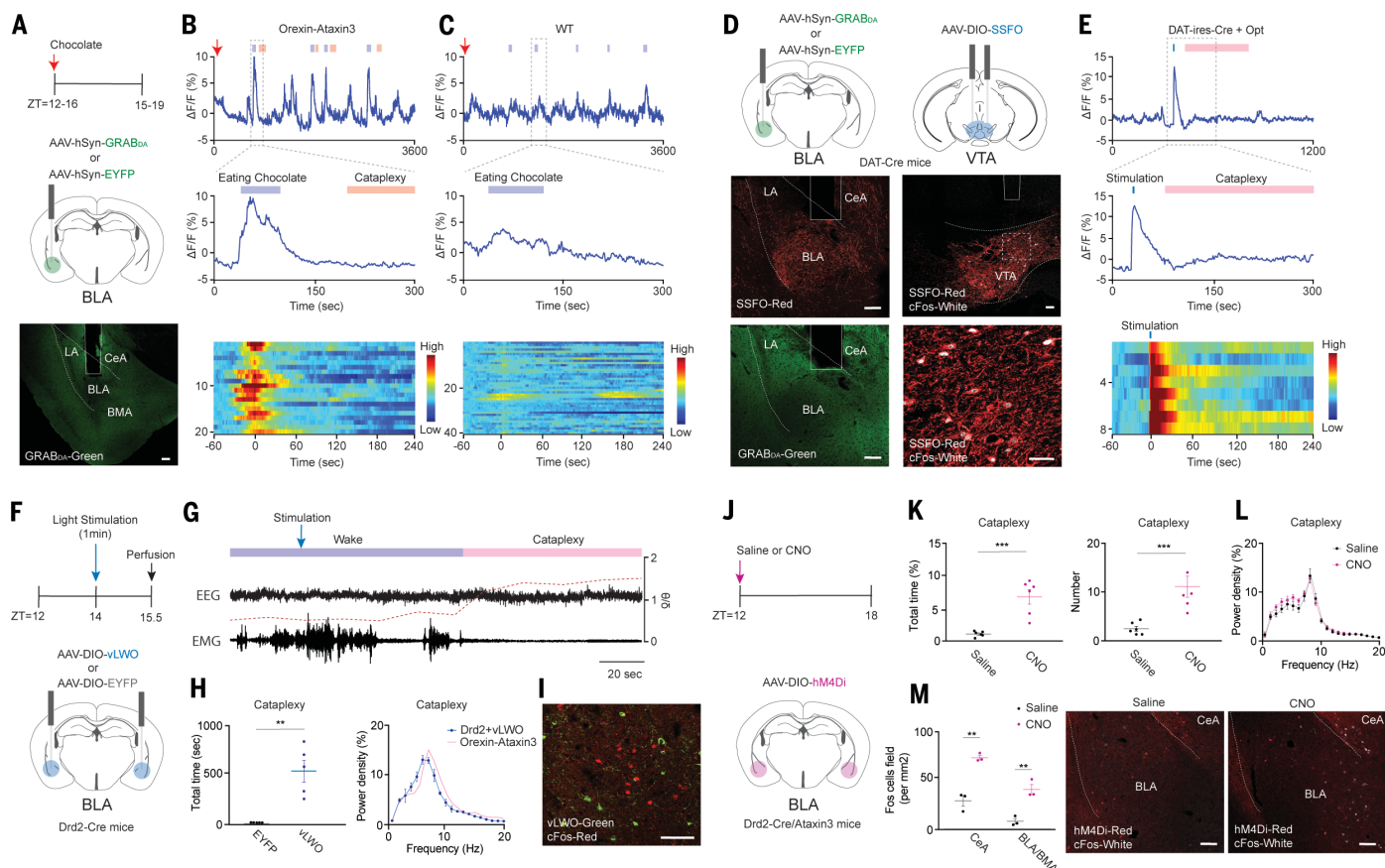


Fig. 5. Transient increase in DA levels in the BLA triggers cataplexy in narcoleptic mice. (A) (Top) Experimental design. Horizontal bar represents time of chocolate feeding. (Middle) Placement of optical fiber and AAV injection. (Bottom) Coronal brain section stained with anti-GFP (green) antibody in the amygdala. The white line marks the position of the optical fiber. Scale bar, 100 μ m. LA, lateral amygdala. (B) (Top) Representative trace of DA level in the BLA in orexin-ataxin 3 mice. Purple and pink bars show times of chocolate feeding and cataplexy, respectively. (Middle) Magnification of time of chocolate feeding and cataplexy. (Bottom) Heatmap showing temporal change of DA levels during chocolate feeding and cataplexy in the BLA in mice ($n = 3$, each recorded three times; total recording number—i.e., number of times of eating chocolate—was 20). (C) (Top and middle) Representative traces of DA levels in the BLA in C57BL/6J mice. Purple bars show times of chocolate feeding. (Bottom) Heatmap showing temporal change of DA levels during chocolate feeding in the BLA in C57BL/6J mice (3 mice, each recorded three times, total recording number = 40). (D) (Top) Placement of optical fiber and GRAB_{DA} and SSFO expression in the BLA and VTA. (Middle and bottom) Coronal brain sections double stained with anti-mCherry (red), anti-GFP (green), or anti-cFos (white) antibodies in the BLA and VTA. The white lines show the positions of the fibers. Scale bars, 100 μ m. (E) (Top) Representative trace of DA level in the BLA in a DAT-ires-Cre mouse before and after optogenetic excitation. Blue bars show time of light stimulation in DA^{VTA} neurons, and pink bars represent time of cataplexy-like episodes. (Middle) Magnification of time of light stimulation and cataplexy. (Bottom) Heatmap showing temporal change of DA levels during cataplexy-like episodes. (F) (Top) Experimental design. Horizontal bar represents time of light stimulation. (Bottom) Location of AAV injection and fiber implantation. (G) Representative traces of EEG and EMG and theta/delta ratio of EEG in a Drd2-Cre mouse expressing vLWO in Drd2-positive cells in the BLA and implanted optical fibers in the BLA (bilateral). The blue arrow shows time of light stimulation, and the purple and pink bars represent wakefulness and cataplexy, respectively. (H) (Left) Total amount of cataplexy episodes. Drd2-Cre mice expressed vLWO or EYFP in the BLA with photostimulation (vLWO, $n = 5$; EYFP, $n = 5$) (relative to EYFP, ** $P < 0.01$, unpaired t test). (Right) Power spectrum of EEG frequency during CLEs evoked by light stimulation compared with that observed during cataplexy in orexin-ataxin 3 mice. (I) Coronal brain section double stained with anti-GFP (green) and anti-cFos (red) antibodies. Scale bar, 100 μ m. (J) (Top) Experimental design. Horizontal bar represents time of saline or CNO administration. (Bottom) Schematic drawing of location of AAV injection. (K) Total amount and number of cataplexy episodes after administration of saline or CNO in ZT12 to ZT18 (relative to saline, *** $P < 0.001$, paired t test). (L) Power spectrum of EEG frequency during cataplexy. (M) (Left) Number of Fos-positive cells in the CeA and the BLA or BMA after administration of saline or CNO (saline, $n = 3$; CNO, $n = 3$) (** $P < 0.01$, unpaired t test). (Right) Coronal brain sections double stained with anti-mCherry (Red) and anti-cFos (white) antibodies in the amygdala. Scale bars, 100 μ m. Data are from Drd2/ataxin 3 mice expressing hM4Di mCherry ($n = 6$).

NREM-to-REM transitions. This is consistent with a study that showed an increase in DA levels in narcoleptic dogs only in the amygdala (30). We previously showed that the activity of 5-HT neurons in the dorsal raphe, which are excited by orexin, is involved in the

suppression of cataplexy (31), which suggests that this pathway might inhibit the release of DA in the BLA through 5-HT-mediated inhibition of DA axonal terminals.

Our study shows the importance of transient DA signaling in the BLA in gating REM

sleep by disinhibiting amygdala neurons that send innervations to REM-regulatory regions (fig. S5). This finding sheds light on the mechanism of cataplexy and on our understanding of the pathophysiology of abnormalities in REM sleep, such as REM sleep behavior

disorder and diseases that involve abnormal DA signaling like Parkinson's disease.

REFERENCES AND NOTES

- T. E. Scammell, E. Arrigoni, J. O. Lipton, *Neuron* **93**, 747–765 (2017).
- C. B. Saper, T. C. Chou, T. E. Scammell, *Trends Neurosci.* **24**, 726–731 (2001).
- L. Dahan *et al.*, *Neuropsychopharmacology* **32**, 1232–1241 (2007).
- J. D. Miller, J. Farber, P. Gatz, H. Roffwarg, D. C. German, *Brain Res.* **273**, 133–141 (1983).
- J. M. Monti, H. Jantos, *Prog. Brain Res.* **172**, 625–646 (2008).
- A. Eban-Rothschild, G. Rothschild, W. J. Giardino, J. R. Jones, L. de Lecea, *Nat. Neurosci.* **19**, 1356–1366 (2016).
- K. T. Beier *et al.*, *Cell* **162**, 622–634 (2015).
- K. T. Beier *et al.*, *Cell Rep.* **26**, 159–167.e6 (2019).
- F. Sun *et al.*, *Cell* **174**, 481–496.e19 (2018).
- O. Yizhar *et al.*, *Nature* **477**, 171–178 (2011).
- Y. Oishi, M. Lazarus, *Neurosci. Res.* **118**, 66–73 (2017).
- K. Dzirasa *et al.*, *J. Neurosci.* **26**, 10577–10589 (2006).
- J. M. Monti, D. Monti, *Sleep Med. Rev.* **11**, 113–133 (2007).
- M. M. S. Lima *et al.*, *Behav. Brain Res.* **188**, 406–411 (2008).
- R. Kumar Yadav, B. N. Mallick, *Neuropharmacology* **193**, 108607 (2021).
- O. A. Masseck *et al.*, *Neuron* **81**, 1263–1273 (2014).
- C. R. Burgess, G. Tse, L. Gillis, J. H. Peever, *Sleep* **33**, 1295–1304 (2010).
- S. Nishino *et al.*, *J. Neurosci.* **11**, 2666–2671 (1991).
- E. Mignot *et al.*, *J. Neurosci.* **13**, 1057–1064 (1993).
- J. Hara *et al.*, *Neuron* **30**, 345–354 (2001).
- Y. Oishi *et al.*, *J. Neurosci.* **33**, 9743–9751 (2013).
- T. E. Scammell, J. T. Willie, C. Guillermault, J. M. Siegel, International Working Group on Rodent Models of Narcolepsy, *Sleep* **32**, 111–116 (2009).
- M. Corsi-Cabrera *et al.*, *J. Sleep Res.* **25**, 576–582 (2016).
- P. Maquet *et al.*, *Nature* **383**, 163–166 (1996).
- J. P. Wisor *et al.*, *J. Neurosci.* **21**, 1787–1794 (2001).
- S. Meletti *et al.*, *J. Neurosci.* **35**, 11583–11594 (2015).
- C. R. Burgess, Y. Oishi, T. Mochizuki, J. H. Peever, T. E. Scammell, *J. Neurosci.* **33**, 9734–9742 (2013).
- M. S. Reid *et al.*, *Brain Res.* **733**, 83–100 (1996).
- M. Okura, J. Riehl, E. Mignot, S. Nishino, *Neuropsychopharmacology* **23**, 528–538 (2000).
- J. D. Miller, K. F. Faull, S. S. Bowersox, W. C. Dement, *Brain Res.* **509**, 169–171 (1990).
- E. Hasegawa *et al.*, *Proc. Natl. Acad. Sci. U.S.A.* **114**, E3526–E3535 (2017).

ACKNOWLEDGMENTS

We thank T. Amano and T. Maejima for valuable discussions.

Funding: This work was supported by JSPS KAKENHI Grant-in-Aid for Scientific Research (B) (JP 18H02595) (to T.S.); JSPS KAKENHI Grant-in-Aid for Scientific Research (A) (JP 21H04796) (to T.S.); JSPS KAKENHI Grant-in-Aid for Scientific Research on Innovative Areas, "Willydynamics" (16H06401) (to T.S.); JSPS KAKENHI grant no. JP19K22465 (to T.S.); JST CREST grant no. JPMJCR1655 Japan (to T.S.); AMED grant no. JP21zf0127005 (to T.S.); JSPS KAKENHI Grant-in-Aid for Young Scientists (18K14846) (to E.H.); Naito Memorial Science Grant/Research Grant 2017 (to E.H.); SENSHIN Medical Research Foundation 2017 Young Researcher Grant (to E.H.); and Takeda Science Foundation 2019 (to E.H.).

Author contributions: Conceptualization: E.H. and T.S. Methodology: E.H., T.S., Y.C., A.M., K.S., and Y.L. Funding acquisition: E.H. and T.S. Project administration: E.H. and T.S. Supervision: T.S. Writing: E.H. and T.S. **Competing interests:** The authors declare that they have no competing interests. **Data and materials availability:** All data are available in the main text or the supplementary materials.

SUPPLEMENTARY MATERIALS

science.org/doi/10.1126/science.abl6618

Materials and Methods

Figs. S1 to S11

Tables S1 to S6

References (32–37)

MDAR Reproducibility Checklist

Movies S1 and S2

View/request a protocol for this paper from Bio-protocol.

29 July 2021; accepted 14 January 2022

10.1126/science.abl6618